Dynamic inversion of the 2000 Tottori earthquake based on elliptical subfault approximations

Sara Di Carli,[1] Caroline François-Holden,[2] Sophie Peyrat,[3] and Raul Madariaga[1]

Received 5 February 2009; revised 20 August 2010; accepted 26 August 2010; published 29 December 2010.

[1] We propose a simplified nonlinear method for the kinematic and dynamic inversion of near-field strong motion data at low frequencies. Using a few elliptical patches we reduce the number of independent parameters of the inverse problem. We apply this method to the dynamic inversion of the Western Tottori (Japan) earthquake (M_w 6.6–6.8) of 6 October 2000. Using unfiltered records we relocated the hypocenter close to 14 km in depth. Fifteen records obtained by the KiK-net and K-NET accelerometer networks were then filtered to the 0.1–0.5 Hz frequency range and integrated to displacement. We compare observed and synthetic records using the $\mathcal{L}^2$ norm. A nonlinear kinematic inversion for the elliptical subfaults is first computed using the neighborhood algorithm (NA). Inversion converges to a slip distribution modeled by just two elliptical patches. We then propose a dynamic inversion method based on the same simple geometrical ideas. Dynamic rupture propagation is computed by finite differences on a coarse numerical grid. Rupture propagation is controlled by a classical slip weakening friction law. Inversion is implemented with the NA for a barrier model. In this model prestress is uniform and rupture propagation is arrested by a simple distribution of barriers. Inversion converges to a model with two elliptical barriers. Synthetics computed for the dynamic inversion fit the observed data, reducing the variance by nearly 60%. By making different assumptions about the rupture process we illustrate the nonuniqueness of the solution to dynamic inversion.

Citation: Di Carli, S., C. François-Holden, S. Peyrat, and R. Madariaga (2010), Dynamic inversion of the 2000 Tottori earthquake based on elliptical subfault approximations, *J. Geophys. Res.*, *115*, B12328, doi:10.1029/2009JB006358.

1. Introduction

[2] To unravel the rupture history of large earthquakes a number of methodologies have been proposed using seismic and geodetic data. Linear and nonlinear kinematic inversions have been used in order to retrieve the details of the rupture process of large earthquakes using both near and far field seismic data. The conventional procedure is to compute synthetic seismograms and compare them to the observed ones searching for the distribution of slip or slip rate on the fault [see, e.g., *Hartzell and Heaton*, 1983; *Cotton and Campillo*, 1995]. Kinematic inversions are very efficient to retrieve source parameters such as slip distribution, rupture velocity and rupture time. Dynamic inversions on the other hand, should generate source models that satisfy well-posed boundary conditions on the fault surface. The forward problem in dynamic inversion consists in computing rupture propagation under the simultaneous control of the initial stress distribution on the fault and rupture resistance modeled by a friction law. Unfortunately, dynamic inversions are expensive and the standard procedure to do kinematic inversion using rectangular slip patches may not be directly used in dynamic inversion.

[3] Several authors have proposed to reconstruct the dynamic stress field from the slip distribution retrieved from kinematic inversion [*Fukuyama and Mikumo*, 1993; *Ide and Takeo*, 1997; *Olsen et al.*, 1997; *Bouchon et al.*, 1998]. This approach has several problems because the kinematic models may not be consistent with any well posed dynamic fracture model. Another problem discussed by *Guatteri and Spudich* [2000] is that since kinematic inversions are nonunique it is difficult to estimate stress and frictional parameters from them. *Peyrat et al.* [2001] did a dynamic inversion of the Landers earthquake of 1992 by a trial and error method. *Peyrat and Olsen* [2004] did a full nonlinear dynamic inversion of the Tottori earthquake using the neighborhood algorithm (NA) proposed by *Sambridge* [1999a, 1999b]. These authors discretized the fault into a checkerboard of rectangular patches of constant stress. This kind of discretization poses a number of problems because of the very large number of patches needed to model the fault, and because of mathematical problems due to stress discontinuities at the border between patches.

[4] Following an idea originally proposed by *Vallée and Bouchon* [2004] for the kinematic inversion of teleseismic

[1]Laboratoire de Géologie, CNRS-ENS, Paris, France.
[2]GNS Science, Lower Hutt, New Zealand.
[3]Institut de Physique du Globe, Paris, France.

0148-0227/10/2009JB006358

Table 1. Velocity Structure

Depth	V_p	V_s	ρ	Q_p	Q_s
0	5.50	3.179	2600	500	200
2	6.05	3.497	2700	500	200
16	6.60	3.815	2800	500	200
38	8.03	4.624	3100	500	200

data, we consider the event as an ensemble of elliptical patches. Since an elliptical patch has a small number of independent degrees of freedom we significantly reduce the number of parameters for the inversion. The elliptical patch method is actually a generalization of the approach proposed by *Backus and Mulcahy* [1976a, 1976b] in order to invert for moments of the slip distributions instead of a grid of rectangular slip patches. This approach has been applied in the past to kinematic inversion by *Gusev and Pavlov* [1988], *Bukchin* [1995] and *McGuire et al.* [2001], among others.

[5] We apply the method of elliptical patches to the 2000 Western Tottori earthquake, an event that was very well recorded by the K-NET and KiK-net networks of NIED (National Research Institute for Earth Science and Disaster Prevention). For this earthquake, a large number of different kinematic inversions have been published. Even if these studies obtain different final slip models, they all are able to reproduce the observed seismograms. *Iwata and Sekiguchi* [2002], *Pulido and Kubo* [2004], *Semmane et al.* [2005], *Piatanesi et al.* [2007] and *Monelli et al.* [2009] showed that most of the slip for this event occurred away from the hypocenter near the free surface.

[6] Dynamic inversion is a major computational challenge, even with a reduced set of parameters as we propose, exploration of the full space of possible models is expensive, or simply impossible. In order to reduce the subset of model space to be explored, we introduced a priori information in dynamic inversion. For that purpose we first did a non linear kinematic inversion based on the use of elliptical subfaults (section 3). From these inversions we find a priori information about the stress fields that may produce these kinematic models. Then the dynamic rupture inversion is implemented using the NA for a barrier model (section 4). Using a linear slip weakening friction law, we invert for a yield (or peak) stress distribution controlled by two elliptical patches. The models obtained by dynamic inversion fit the data just as well or better than the models we obtained by kinematic inversion (section 5). The solutions are also nonunique. We conclude with a limited exploration of the subspace of dynamic models that satisfy the observations.

2. The 2000 Tottori Earthquake

2.1. Hypocenter Location

[7] On 6 October 2000 at 4:30:25.3 GMT, the western Tottori Earthquake (M_w 6.7) occurred on a left-lateral strike-slip fault in western Honshu, Japan. The epicenter was located at 35.269 N and 133.357 E [*Iwata and Sekiguchi*, 2002]. The event was characterized by the absence of surface rupture and a poorly constrained hypocentral depth. Depths vary from 7.8 km [*Iwata and Sekiguchi*, 2002] down to 15.0 km (Harvard, CMT). The Tottori earthquake was recorded by high-resolution strong motion networks (K-NET and KiK-net) operated by the National Institute for Earth Sciences and Disaster Prevention (NIED). Since these data have absolute timing, we relocated the hypocenter directly from raw near field records. On the raw data, we could clearly identify the arrival of P waves from the first event. Using the velocity structure proposed by *Dalguer et al.* [2002] (Table 1), we relocated the hypocenter close to 14 km in depth, in agreement with *Pulido and Kubo* [2004] and with the relocation of aftershock sequences by *Fukuyama et al.* [2003]. This velocity model was used for the hypocenter determination by the Research Center for Earthquake Prediction-Disaster Prevention Research Institute (RCEP-DPRI), Kyoto University. We approximated the earthquake as a pure strike-slip event on a single, planar, vertical segment of azimuth 150°, dip 90°, and rake 0°.

2.2. Data Processing

[8] For the kinematic and dynamic inversion we used data from all three components of a set of 15 strong motion recordings located within 50 km of the epicenter of the Tottori earthquake. The stations and the fault trace are shown in Figure 1. We used the absolute time contained in the digital recordings in order to align the data to a common starting time of 13:30:18 GMT in agreement with the origin time adopted by *Iwata and Sekiguchi* [2002] and *Semmane et al.* [2005]. The data and synthetic displacement time histories were band-pass filtered between 0.1 and 0.5 Hz with a causal Butterworth filter. In this frequency band the K-NET and KiK-net records have the same waveform. The causal filter produces a small frequency-dependent phase shift in the processed data but the main features of the records were well preserved. Synthetics will be processed with the same filter so that the phase shift is the same in observed and synthetics.

3. Kinematic Inversion Method

[9] Before attempting dynamic inversion, we did a kinematic inversion in order to determine the overall characteristics of the kinematic models based on the same elliptical patch approximation that will be used in dynamic inversion. Kinematic inversion at low frequencies provides an overall view of the rupture process of the earthquake, its slip distribution and rupture times. As we will promptly discuss we use these properties as a priori information in dynamic inversion. We searched for model comprising several elliptical patches on a fault plane of 32 × 32 km. After several trial-and-error essays it turned out that only two ellipses could be resolved. For three or more ellipses the inverse problem did not converge in reasonable time. Even for two ellipses, some parameters are not well resolved, an indication that the inverse kinematic problem is nonunique even for two patches.

3.1. Forward Kinematic Model

[10] We assume that the slip distribution D measured from the center of an ellipse has the Gaussian distribution

$$D(x,y) = D_m \exp -\left(x^2/a^2 + y^2/b^2\right), \quad (1)$$

where D_m is the maximum amplitude in the elliptical patch of semiaxes a and b. The slip distribution is continuous but concentrated inside the ellipse of semiaxes a and b. This slip

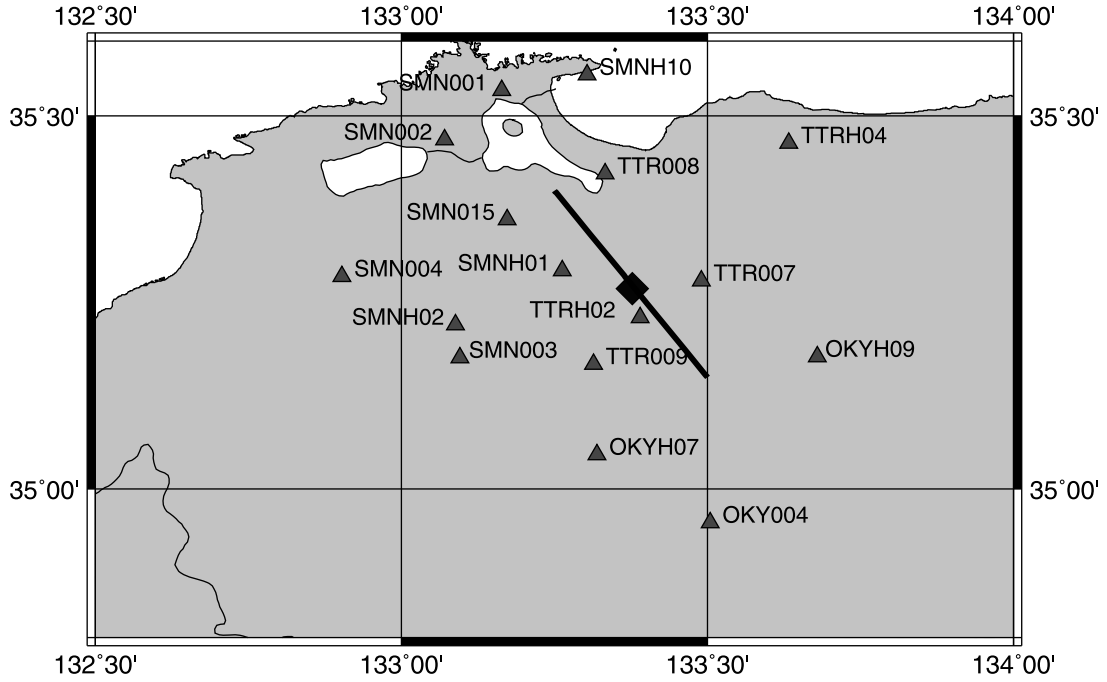

Figure 1. Map of the location of the 6 October 2000 Tottori earthquake (diamond) and the sites of the 15 accelerometers (triangles) that we used for kinematic and dynamic inversion. The thick line is an approximation to the trace of the almost vertical strike-slip fault on which the earthquake occurred.

function is inspired by the moments of order 2 of slip distributions proposed by *Backus and Mulcahy* [1976a, 1976b] and applied to several earthquakes by *Gusev and Pavlov* [1988], *Bukchin* [1995] and *McGuire et al.* [2001].

[11] In every patch, rupture speed was assumed to be constant and the time of rupture t_r was computed with respect to distance from the hypocenter in order to insure causality in the forward models. More complex rupture propagation with variable speed could be easily implemented, but our data did not require such complexities.

[12] Slip rate on every patch was also very simple. The source time function at any point on the fault was a triangular function of duration $\tau = 1$ s around the rupture time t_r. Other source time functions were studied but we did not observe any obvious effect on the convergence of kinematic inversion.

[13] In the forward model, every elliptical patch is described by 7 parameters: two coordinates of the center, two semiaxes a and b, an angle of orientation ϕ, slip amplitude D_m and rupture speed v_r. Risetime $\tau = 1$ was fixed in the kinematic inversion.

[14] The discrete wave number AXITRA code of *Cotton and Coutant* [1997] was employed to simulate wave propagation. The fit between observed (obs) and synthetic (synth) records was measured with the $\mathcal{L}^2$ norm:

$$\mathcal{L}^2 = \frac{\sum_i (\text{obs} - \text{synth})^2}{\sum_i (\text{obs})^2}, \qquad (2)$$

where the index i runs over all samples in every seismogram considered in the inversion.

3.2. Neighborhood Algorithm

[15] The neighborhood algorithm (NA) of *Sambridge* [1999a, 1999b] was chosen to search for the minimum wavefit error $\mathcal{L}^2$. This is a nonlinear derivative-free method employing geometrical concepts to guide a direct search in the parameter space. This parameter space is partitioned into a set of Voronoi cells, each cell being associated with one model. At every iteration, a set of models is recalculated in the Voronoi cells of the previous set with the smallest misfit. The neighborhood algorithm requires only two control parameters: the sample size of each iteration n_s and the number of cells n_r in which a new sample is searched. To summarize the inversion technique: (1) The n_s models are distributed uniformly into the space of parameters generated. (2) For each model synthetics seismograms are computed and the n_r models with smallest misfit are selected. (3) A random set of new models is generated in the Voronoi cells of the best n_r models and the process is restarted.

3.3. Inversion Results

[16] We present here only the best kinematic model we could find. Many models were generated in our search for a minimum and they can be exploited to study the resolution of inversion. Since our goal was to estimate the range of parameters that produce good kinematic fit we will not study the nonuniqueness of kinematic inversion. We refer to *Peyrat et al.* [2001] for a study of nonuniqueness in the kinematic inversion of an earthquake in northern Chile.

3.4. Slip Distribution

[17] The NA algorithm for kinematic inversion converged in 4000 iterations. Figure 2 shows convergence as a function of iteration number. Convergence of kinematic inversion was very fast, the search algorithm rapidly found a small area of model space. The slip distribution and the rupture time as a function of position on the fault for the best model are shown in Figure 3. Rupture is characterized by a small

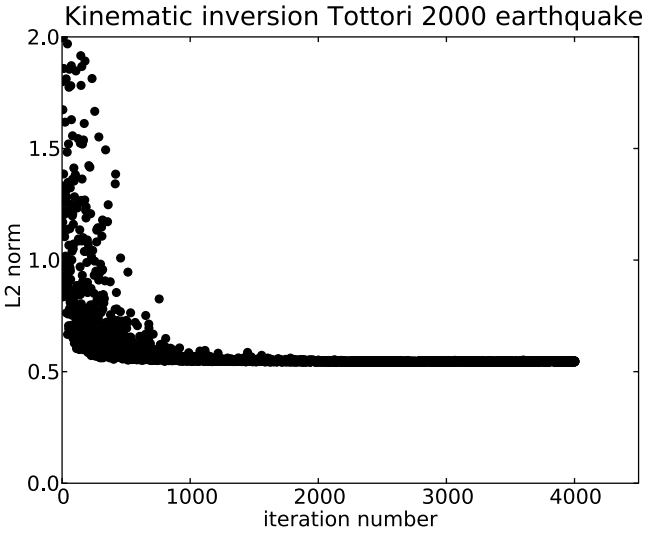

Figure 2. Kinematic inversion. Plot of the $\mathcal{L}^2$ misfit function between synthetics and observations as a function of iteration number during the kinematic inversion by the neighborhood algorithm of *Sambridge* [1999a, 1999b].

elliptical patch of maximum slip D_m = 1 m and rupture velocity 1.91 km/s near the hypocenter. A second larger patch was located above the hypocenter, close to the free surface, with maximum slip of 2.25 m and rupture velocity 2.15 km/s. This model had a seismic moment $M_0 = 1.15 \times 10^{19}$N m ($M_w = 6.64$), which is within the range of moments obtained by *Semmane et al.* [2005] (1.6×10^{19}N m), *Peyrat and Olsen* [2004] (9.3×10^{18}N m) and *Yagi and Kikuchi* [2000] (1.1×10^{19}N m).

3.5. Waveform Fits

[18] In Figure 4 we compare the observed and synthetic records for the best solution of the inverse kinematic problem. Both observed and synthetic records were processed with the same two-pole causal Butterworth filter in the frequency range from 0.1 to 0.5 Hz. We obtain a very good overall fit of the seismograms for all components. The relative error computed from model A was $\mathcal{L}^2 = 0.54$. At some stations there remain waveform details that were not fully modeled, particularly for stations OKYH07 and TTR009 in the EW component. We obtain generally a better fit for the stations situated near the fault (SMN015, SMNH01, TTR008 and TTR009). An earlier inversion with only the 8 closest stations produced a much better fit: $\mathcal{L}^2 = 0.29$. There are many reasons why stations closer to the fault are better modeled, for instance, inadequacies in the elastic model of Table 1, less scattering and better sensitivity to the details of rupture.

4. Dynamic Inversion Method

[19] In previous attempts to dynamic inversion, *Peyrat et al.* [2001] and *Peyrat and Olsen* [2004] used a grid of rectangular stress patches to describe the initial stress field and the distribution of friction on the fault surface. Although this method led to successful solutions, there are several problems that need to be carefully considered. First, the rectangular patches produce strong stress singularities at the edge of the patches. These singularities appear in the stress components that are not directly inverted for. Their effect on rupture propagation is not clear to us. Second, in order to reduce the effect of these spurious stresses some scheme must be devised in order to smooth numerical solutions. Third, a large number of rectangular patches are needed to properly simulate the variability of stress and friction on the fault plane. As a consequence, the inversion contains a large number of degrees of freedom making it very expensive even for simple source models. Fourth, the implementation of rectangular patches does not have a simple mechanism to stop rupture propagation, so that many of the models generated by the inversion algorithm do not stop and therefore do not satisfy the data. Most of these difficulties can be

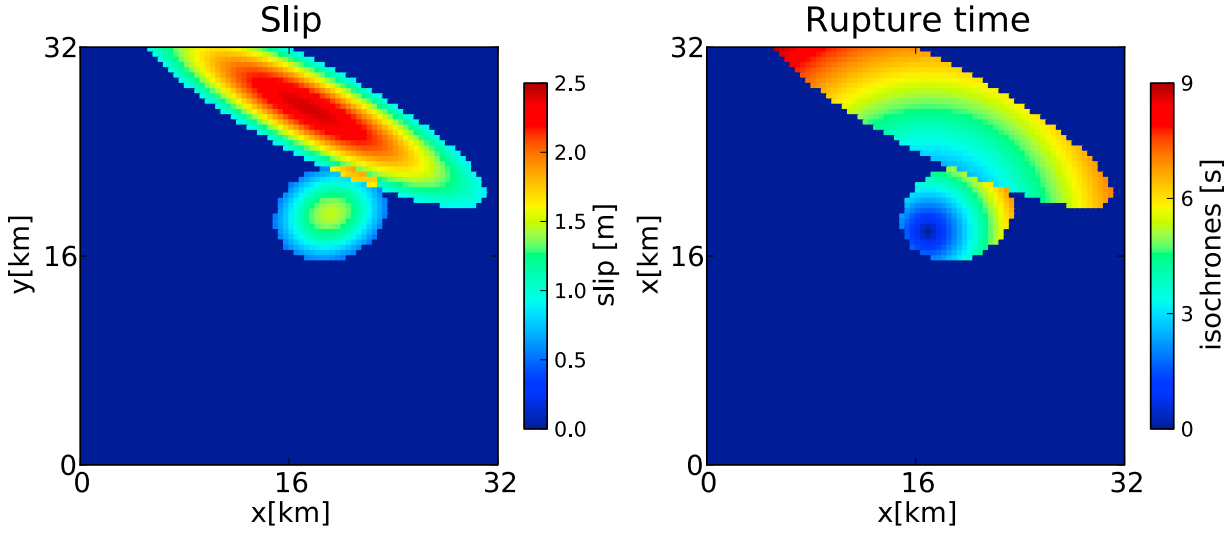

Figure 3. Kinematic inversion. (left) Slip distribution and (right) rupture time for best kinematic model found in the nonlinear kinematic inversion of the 6 October 2000 Tottori earthquake. This model has an $\mathcal{L}^2$ norm of 0.51.

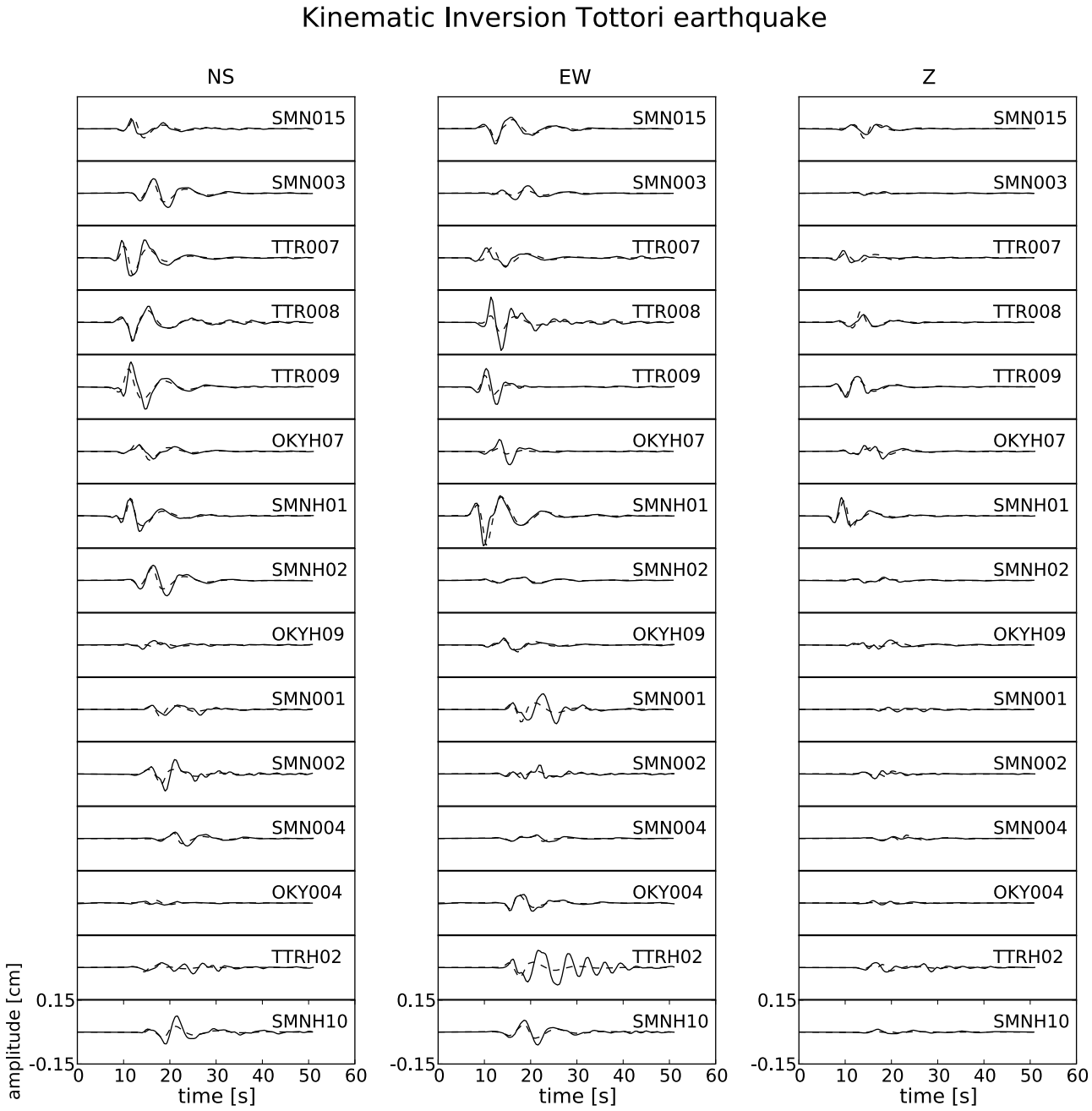

Figure 4. Kinematic inversion. Comparison of the three components of the displacement field produced by the Tottori earthquake (continuous line) and the synthetics computed for the best kinematic model of the earthquake shown in Figure 3. The misfit was $\mathcal{L}^2 = 0.54$. Data was integrated from accelerograms and filtered in the band pass 0.1–0.5 Hz.

avoided by using smooth distributions of stress and rupture resistance with localized barriers that may stop rupture. Such distributions may be easily defined using the elliptical patch technique proposed by *Vallée and Bouchon* [2004].

4.1. Barrier Model and Dynamic Simulation

[20] Two important problems arise in dynamic inversions. The first is that dynamic source parameters are often difficult to estimate because of their strong nonlinearity [*Guatteri and Spudich*, 2000]. The second problem is that the inverse dynamical problem is intrinsically ill posed: we can look for solutions of barrier or asperity type [*Madariaga*, 1979]. In the ideal asperity model of *Kanamori and Stewart* [1978] only the initial stress field is heterogeneous. The fault presents some regions of high concentration of stress field where the rupture starts and propagates. In the ideal barrier model of *Das and Aki* [1977] only the parameters of the friction law are heterogeneous. The fault presents some regions (barriers) where the rupture cannot penetrate. *Peyrat et al.* [2001] modeled the dynamic rupture of the 1992 Landers earthquake with a trial-and-error method with these two complementary models, the barrier

Table 2. Inversion of the Tottori Earthquake: Model A

Parameter	Minimum Value	Maximum Value	Inversion
a1	4.000	10.000	9.994
b1	2.000	7.200	6.003
x1	12.000	22.000	21.235
y1	10.000	18.000	14.175
phi1	0.320	0.720	0.322
a2	8.000	12.000	9.305
b2	3.200	8.000	5.352
x2	14.000	22.000	16.827
y2	2.000	6.000	2.030
phi2	0.040	0.440	0.127

and the asperity model. They showed that both models successfully fit the rupture history and the duration of this earthquake, confirming the earlier conjecture that seismic data cannot distinguish between barriers and asperities [*Madariaga*, 1979]. The real solution must then be somewhere between these two models, but this cannot be determined from seismic data alone.

[21] For dynamic inversion, it should be very important to test both the barrier and asperity source models. We did some trial and error dynamic inversions for the Tottori earthquake concluding that the barrier model was easier to implement. For this reason, in this first attempt to do dynamic inversion we decided to study only the ideal barrier model. For the appropriate implementation of asperity models it is necessary to define initial stress functions with sharp negative stress drop surrounding the rupture area. Without these negative stress drop zones, rupture would not stop. More work is needed to implement such a model.

[22] For dynamic modeling we used the slip weakening friction law proposed by *Ida* [1972]:

$$\begin{aligned} T_f(D) &= T_u\left(1-\tfrac{D}{D_c}\right) \qquad \text{for } D < D_c \\ T_f(D) &= 0 \qquad\qquad\qquad\quad \text{for } D > D_c, \end{aligned} \tag{3}$$

where $T_f(D)$ is friction as a function of slip D. T_u is the peak frictional stress and D_c the slip-weakening distance. In the inversions we assumed a constant slip weakening distance D_c because its value is limited by the accuracy of the finite difference method. We controlled the rupture process with the distribution of the heterogeneous peak stress T_u. We model the distribution of T_u (x,y) with two elliptical patches of constant yield stress T_u. The exterior of the ellipses is unbreakable, so that rupture can propagate only inside the elliptical patches. This corresponds to the ideal barrier model as defined by *Das and Aki* [1977] and *Aki* [1979]. For each elliptical patch, six parameters describe the distribution of the yield stress T_u: two coordinates of the center of the ellipse, two principal semiaxes, the rotation angle with respect to horizontal and the peak stress level T_u.

[23] The forward problem of the spontaneous dynamic rupture propagation for a vertical strike slip fault embedded in a 3-D elastic medium was solved using a fourth-order staggered-grid finite difference (FD) method [*Madariaga et al.*, 1998]. We used thin boundary conditions at the fault. The hypocentral depth and velocity structure are the same as for the kinematic model. Our scheme includes free surface boundary conditions and absorbing boundaries in the internal grid boundaries. We used grid steps of 400 m and time steps of 0.02 s in order to ensure accuracy of the results. The grid size was 80 × 80 × 80 so that the fault plane had a total size of 32 × 32 km^2.

[24] In agreement with the barrier model, the initial stress field T_e was assumed to be uniform everywhere except in a small asperity located at the hypocenter. The initial stress at the asperity is $T_{asp} = T_u$ and its radius was r = 1.6 km. This asperity satisfies the Griffith criterion for rupture initiation so that is ready to break [see, e.g., *Madariaga and Olsen*, 2000].

4.2. A Priori Constraints for Dynamic Inversion

[25] Ideally, in the inverse dynamic problem we should invert for all the parameters of the friction law, but these parameters are in fact not independent. The rupture models that produce acceptable synthetics must satisfy at least two constraints. First, they must satisfy the extended Griffith criterion [*Madariaga and Olsen*, 2000]. This criterion is derived from the nondimensional number

$$\kappa = \frac{T_e^2}{\mu T_u}\frac{L}{D_c}, \tag{4}$$

where L is a characteristic size of the rupture and the other parameters were already defined. For the elliptical patches we study here a good approximation to L is the semi minor axis b of each ellipse. Since κ must be very close to critical for rupture to be subshear, the values of T_u, T_e, and D_c are not independent. If κ is subcritical rupture will not extend beyond the initial asperity; if it is about 1.2 times critical, rupture will become supershear. In our numerical simulations D_c = 0.8 m because this is the minimum value that is

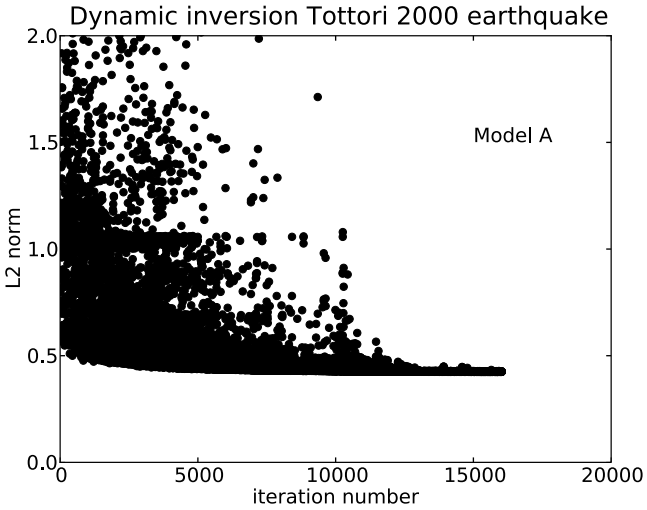

Figure 5. Dynamic inversion for model A. Plot of the $\mathcal{L}^2$ misfit function between synthetics and observations as a function of iteration number during the dynamic inversion by the neighborhood algorithm of *Sambridge* [1999a, 1999b]. Data was integrated from accelerograms and filtered in the band pass 0.1–0.5 Hz. Models with misfit much greater than 1 correspond to ruptures with moments and durations much larger than those observed. The models concentrated near misfit equal to 1 are frustrated models that did not propagate because κ was subcritical. The minimum misfit was $\mathcal{L}^2$ = 0.399, and the total number of models generated by inversion was 16,032.

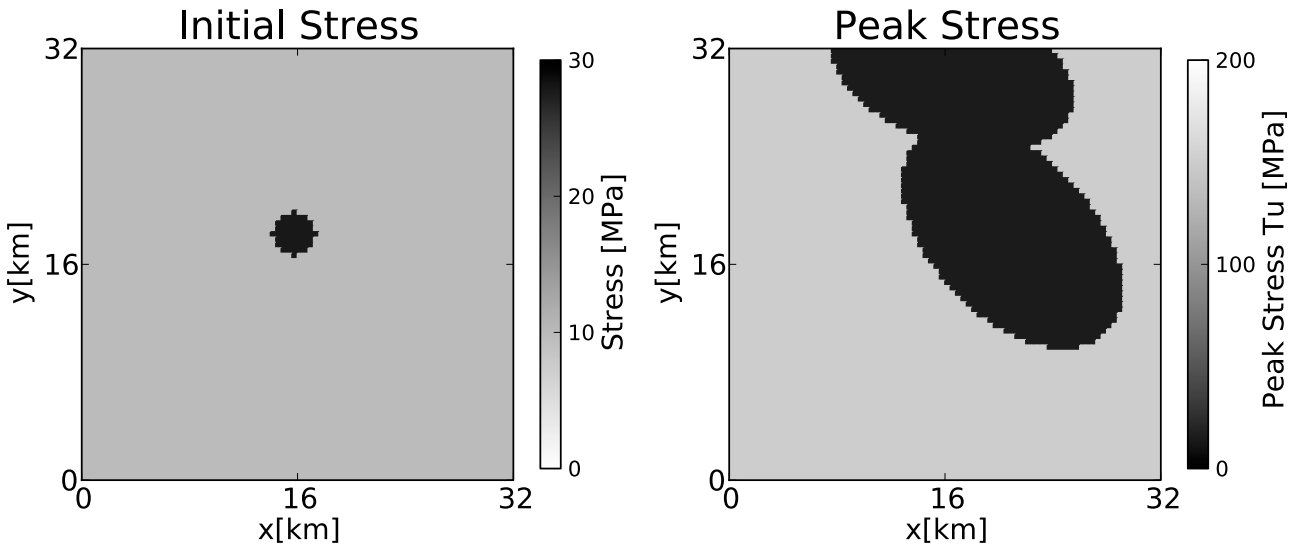

Figure 6. Dynamic inversion for model A showing (left) initial stress distribution T_e and (right) peak stress T_u rupture time for the best dynamic model found by the nonlinear dynamic inversion of the 6 October 2000 Tottori earthquake. This model has a $\mathcal{L}^2$ norm of 0.399.

compatible with the grid size of our numerical simulation (400 m). We can thus only change the ratio of stresses or the size of the fault so that κ remains close to critical. Dynamic models must also satisfy an additional constraint: that the seismic moment of the model be the same as the observed one. Moment is proportional to $T_e L^3$, so that eligible dynamic models must simultaneously satisfy two a priori constraints: that κ is close to critical and that moment is close to the observed one.

[26] Starting from the fault geometry retrieved from kinematic inversion reported in section 3, we did a series of tests of the forward problem. From these tests we found that T_u = 15 MPa, D_c = 0.8 m and T_e = 10 MPa produced dynamic models that were very close to the results of kinematic inversion. The moment was the same, the rupture duration (controlled by κ) and the slip distribution were very similar to those of the kinematic model. Ideally, we should be able to find models that satisfy moment and κ constraints with the nonlinear inversion algorithm. This is unfortunately not possible with our present computer power because the nonlinear algorithm will explore many models that either do not propagate at all (κ is too small), break the fault too fast (κ is too large) or do not satisfy the moment constraint. We used the values of initial stress and friction mentioned above as a priori constraints in the inversion. Let us remark that these constraints are only used to reduce the size of the parameter space explored by the inversion algorithm in order to make the inverse problem feasible in current computers.

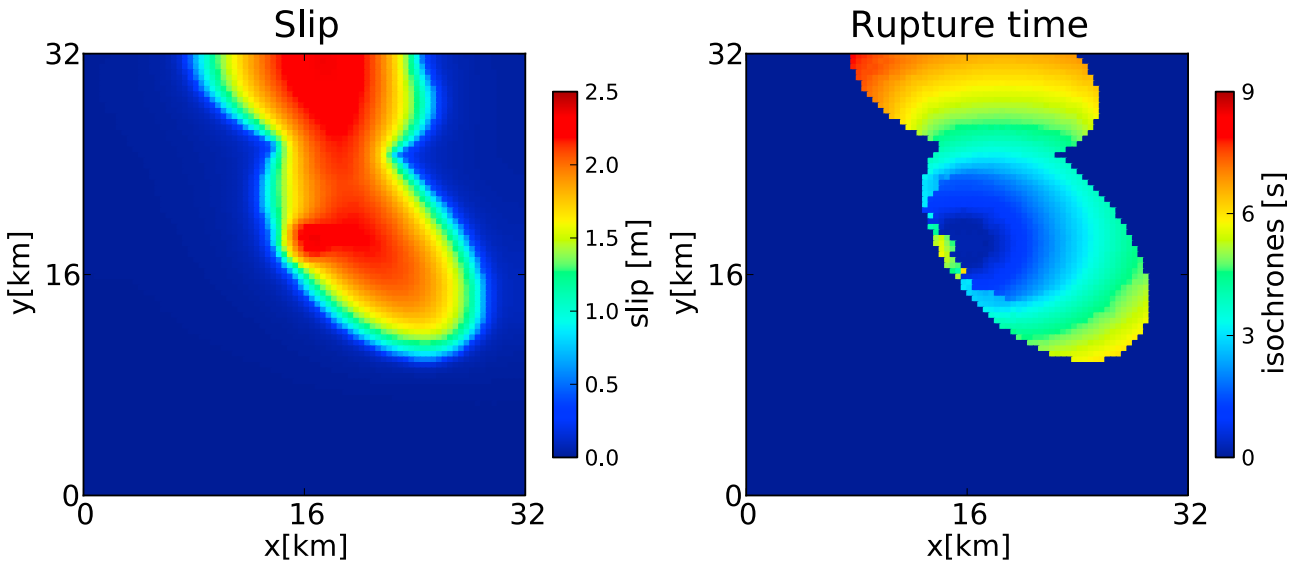

Figure 7. Dynamic inversion for model A showing (left) slip distribution and (right) rupture time for the best dynamic model found by the nonlinear dynamic inversion of the 6 October 2000 Tottori earthquake. This model has a $\mathcal{L}^2$ misfit of 0.399.

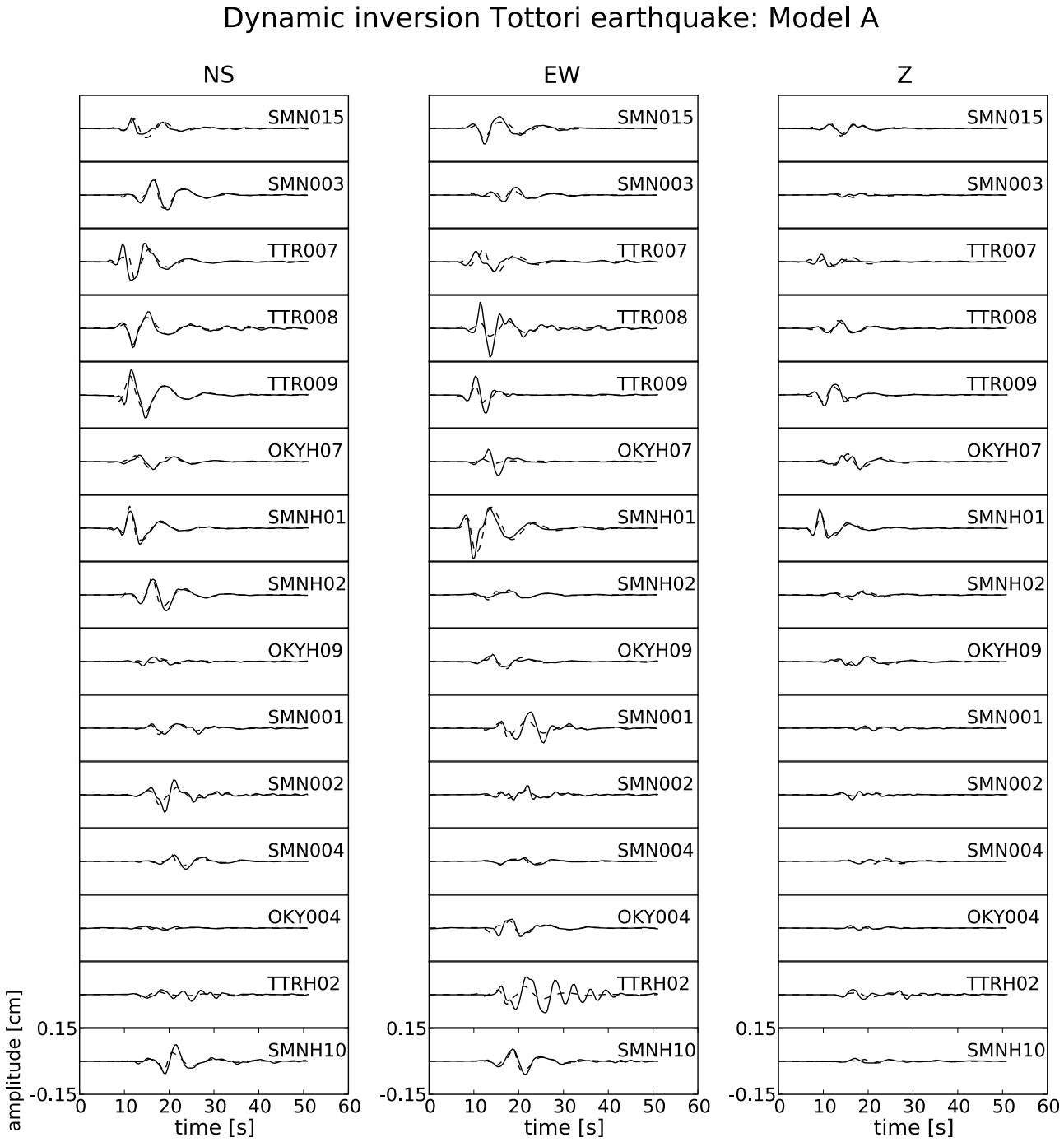

Figure 8. Dynamic inversion for model A. Comparison of the three components of the displacement field produced by the Tottori earthquake (continuous line) and the synthetics computed for the best dynamic model of the earthquake shown in Figures 6 and 7. The misfit was $\mathcal{L}^2 = 0.399$. Data was integrated from accelerograms and filtered in the band pass 0.1–0.5 Hz.

[27] In order to reduce the cost of the solution of the direct problem we used finite difference simulations only to generate the slip rate distribution as a function of time on the fault. Then we generated the synthetic ground motion from slip rate using the discrete wave number method of *Bouchon* [1981]. The particular implementation is the program AXITRA described by *Cotton and Coutant* [1997], in which the reflection-transmission matrices of *Kennet and Kerry* [1979] are used. The fit between observed and synthetics was computed by (2).

5. Inversion Results

[28] We did two separate dynamic inversions that we designated models A and B. The main difference between

Table 3. Inversion of the Tottori Earthquake: Model B

Parameter	Minimum Value	Maximum Value	Inversion
a1	6.880	8.120	8.118
b1	5.440	6.000	5.691
x1	18.400	21.960	19.558
y1	11.600	14.080	12.453
phi1	0.400	0.560	0.400
a2	9.080	11.520	11.497
b2	3.640	4.760	3.650
x2	16.040	22.080	19.002
y2	3.680	5.720	3.773
phi2	0.040	0.080	0.073

them is the range of parameters that we chose for the inversion. Model A had a range of parameters that was much larger than that of model B, yet the two have very similar misfit $\mathcal{L}^2$. This is one way of showing that the dynamic inverse problem has a nonunique solution. In the future, once computer resources permit it, we will do a Monte Carlo search around the optimum model in order to find a set of models that satisfy the observations within a certain margin of error.

5.1. Model A: The Best Dynamic Model

[29] Let us first discuss the best overall model found by the dynamic inversion. We call this model A. For this model we explore 10 parameters, listed in Table 2. These are the principal semiaxes of the ellipses (a and b), the position of the ellipse with respect to the hypocenter (x,y) and the angle ϕ of the principal axis. The indices 1 and 2 refer to each ellipse. As shown in Table 2 the range over which each parameter could vary was large leading to a very large set of potential models. In Figure 5 we show the global convergence of the NA algorithm for model A. In this plot, models with $\mathcal{L}^2$ close to 1 correspond to the models that do not propagate because κ is too small or the ellipses are disjoint so that rupture stops very rapidly after leaving the asperity. The algorithm visits a large number of such models during the initial steps. There are also many models for which $\mathcal{L}^2$ is much larger than 1, over predicting the observed seismograms. The NA algorithm starts to converge after about 11,500 models settling around the minimum values listed in the inversion column of Table 2. The value of the misfit for the best model A was $\mathcal{L}^2 = 0.399$. Comparing the convergence of the kinematic and dynamic inversions we observe that the dynamic ones converge slowly because there are many models that do not fit the seismograms, either because they do not propagate over the whole fault or because they run too fast or produce very large seismic moments.

[30] The distribution of the initial stress and peak stress obtained by NA for model A is shown in Figure 6. The slip distribution produced by this model is shown in Figure 7 (right) and the rupture isochrones (time to rupture of a point on the fault) are shown in Figure 7 (left). We observe that compared to the kinematic model of Figure 3, the elliptical patches of model A are less elongated than those obtained by kinematic inversion. Also the first ellipse of model A is much bigger than that of the best kinematic model. The rupture times computed for the best dynamic model have a similar duration to those of the kinematic solutions. Rupture propagates slowly in the lower central part of the fault near the hypocenter and it accelerates in the second elliptical patch until it breaks the surface. This model agrees with those from most kinematic results: small amount of slip near the hypocenter increasing gradually toward the surface [*Pulido and Kubo*, 2004; *Semmane et al.*, 2005; *Iwata and Sekiguchi*, 2002].

[31] The synthetic and observed seismograms generated by model A are shown in Figure 8. We observe that the general fit is quite satisfactory, actually the fit of the dynamic model (0.399) is better than that of the kinematic synthetics (0.54) shown in Figure 4. We attach no particular significance to this difference because we did not explore

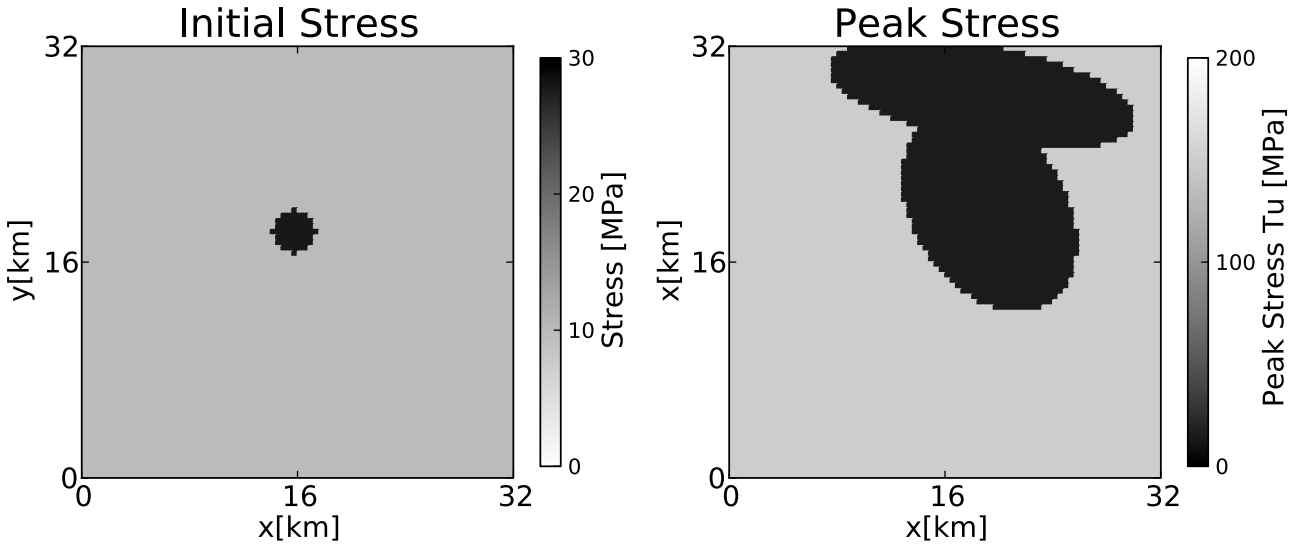

Figure 9. Dynamic inversion for model B showing (left) initial stress distribution T_e and (right) peak stress T_u for the best dynamic model found by the nonlinear dynamic inversion of the 6 October 2000 Tottori earthquake. This model has a $\mathcal{L}^2$ misfit of 0.424.

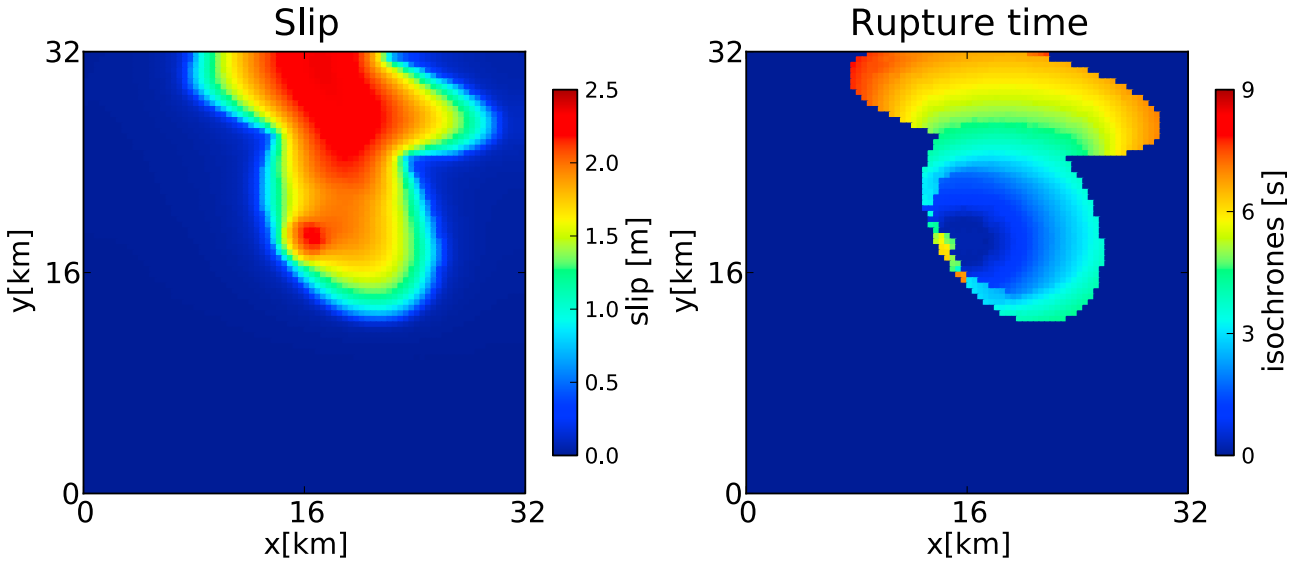

Figure 10. Dynamic inversion for model B showing (left) slip distribution and (right) rupture time for the best dynamic model found by the nonlinear dynamic inversion of the 6 October 2000 Tottori earthquake. This model has a $\mathcal{L}^2$ misfit of 0.424.

kinematic models with variable speeds, a common feature to all the successful dynamic models (see Figure 7, right).

5.2. Model B: A Model That Does Not Break the Surface

[32] Studying the suite of models that are generated by the neighborhood algorithm as it converges (Figure 5) we found that it visited several areas of parameter space where the misfit function $\mathcal{L}^2$ was small. By design the NA abandons those models as it looks for a global minimum. We used that information to find models that do not break the surface. The parameter range explored in this second inversion is listed in Table 3, a subset of the parameter space explored in the inversion for model A. The result of our search is model B listed also in Table 3. The distribution of initial and peak stress inverted for model B is shown in Figure 9. The slip distribution produced by this model is shown in Figure 10 (left) and the time to rupture is shown in Figure 10 (right). The synthetic and observed seismograms generated by model B are shown in Figure 11. Model B fits the data with an error of $\mathcal{L}^2 = 0.424$, that is it is only 10% larger than the misfit of model A. We observe that the main difference between models A and B is the size of the second elliptical patch: in model A the rupture breaks the surface, while in model B the rupture stops very close to the surface. This model, that has less slip near the surface, is more realistic since no surface rupture was observed for the Tottori earthquake.

[33] We observe that the two dynamic models generate displacement time histories that provide a good fit to the observed records. We think that the main features of the low-frequency ground motion (both amplitude and waveforms) have been captured by the synthetic seismograms of Figures 8 and 11. These two dynamic models fit observed records better than the kinematic model of section 3. It is important to recall that, as we already mentioned, these models are members of a larger family of dynamically correct models. These models can be generated by trade off between the stress ratio T_e^2/T_u and the size of the fault. Models A and B illustrate the nonuniqueness of dynamic inversion and the trade offs between different models.

6. Discussion

6.1. Values of the Dynamic Parameters

[34] As discussed previously we decided to use strong a priori constraints in dynamic inversion, fixing the values of T_u, T_e, D_c and T_{asp}. We obtained these values from a small number of forward models based on the kinematic inversion of section 3. These models have slip and slip rate distributions that are in broad agreement with the moment, duration and slip distribution of the kinematic model inverted earlier. From these simulations we found that an initial uniform stress field of T_e = 10 MPa was needed to generate a slip distribution similar to that of the kinematic model. Then we adjusted the friction law so that the total rupture time agreed with that of the kinematic inversion. We found that with peak stress inside the elliptical patches equal to T_u = 15 MPa and slip weakening distance D_c = 0.8 m we obtained reasonable duration. We used this method to reduce the space of parameters and therefore diminish the number of numerical simulations required by dynamic inversion. Letting the nonlinear inversion algorithm search simultaneously for geometry and stress without any a priori constraint is possible but in that case the NA algorithm will visit a very large number of models that either do not propagate, propagate too fast or have incorrect values of seismic moment. Other less strict a priori constraints can be used, but they also require much greater computer resources.

[35] The preferred dynamic models of the Tottori earthquake have a maximum slip of 2.5 m and 2 m for models A and B, respectively. Stress drop in the source area was 10 MPa. This is a rather large value due to the relatively small size of the main elliptical patch. This value of stress drop is actually very similar to those estimated by *Dalguer*

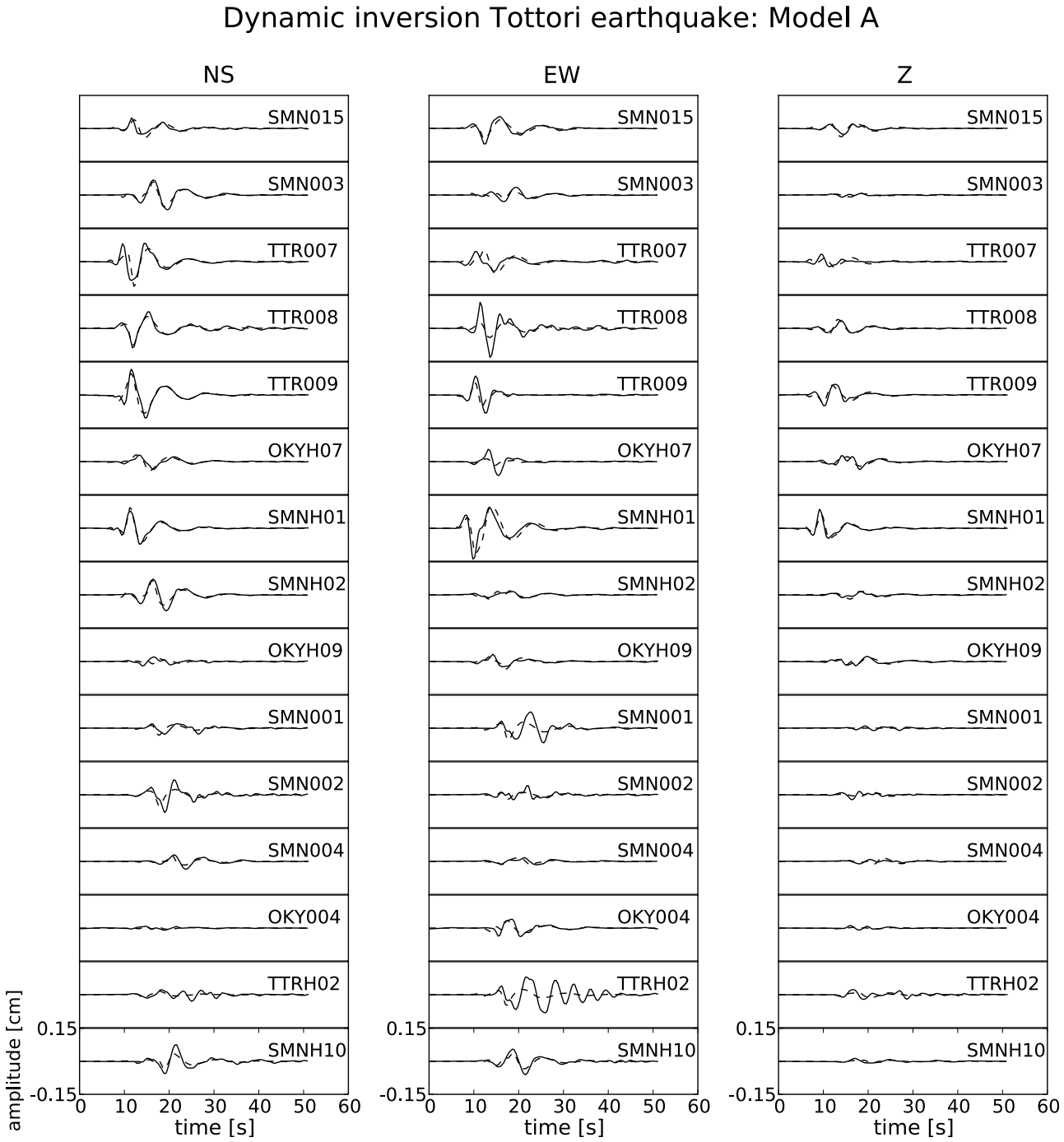

Figure 11. Dynamic inversion for model B. Comparison of the three components of the displacement field produced by the Tottori earthquake (continuous line) and the synthetics computed for the best dynamic model of the earthquake shown in Figures 9 and 10. The misfit was $\mathcal{L}^2 = 0.424$. Data was integrated from accelerograms and filtered in the band pass 0.1–0.5 Hz.

et al. [2002] and *Mikumo et al.* [2003] from kinematic inversions.

[36] Our inversions give a good fit for a slip weakening distance D_c of 0.8 m and a peak stress $T_u = 15$ MPa. This are somewhat large for an earthquake of M_w 6.6. Energy release rate, estimated from these values is $G_c = 6$ MJ/m^2 for model A and the total rupture energy spent by the earthquake was 12.6×10^8 MJ. Using a completely different method, *Mikumo and Fukuyama* [2006] estimated the energy release rate of the Tottori earthquake as 2.5×10^8 MJ and a near-source energy of the order of 5.9×10^8 MJ. These are of the same order of magnitude as our estimates. The rupture process of our best models is quite similar to that found by *Peyrat and Olsen* [2004], with rupture moving gradually toward the upper edge of the fault plane. They found a maximum slip of 2 m that is similar to that of our solution.

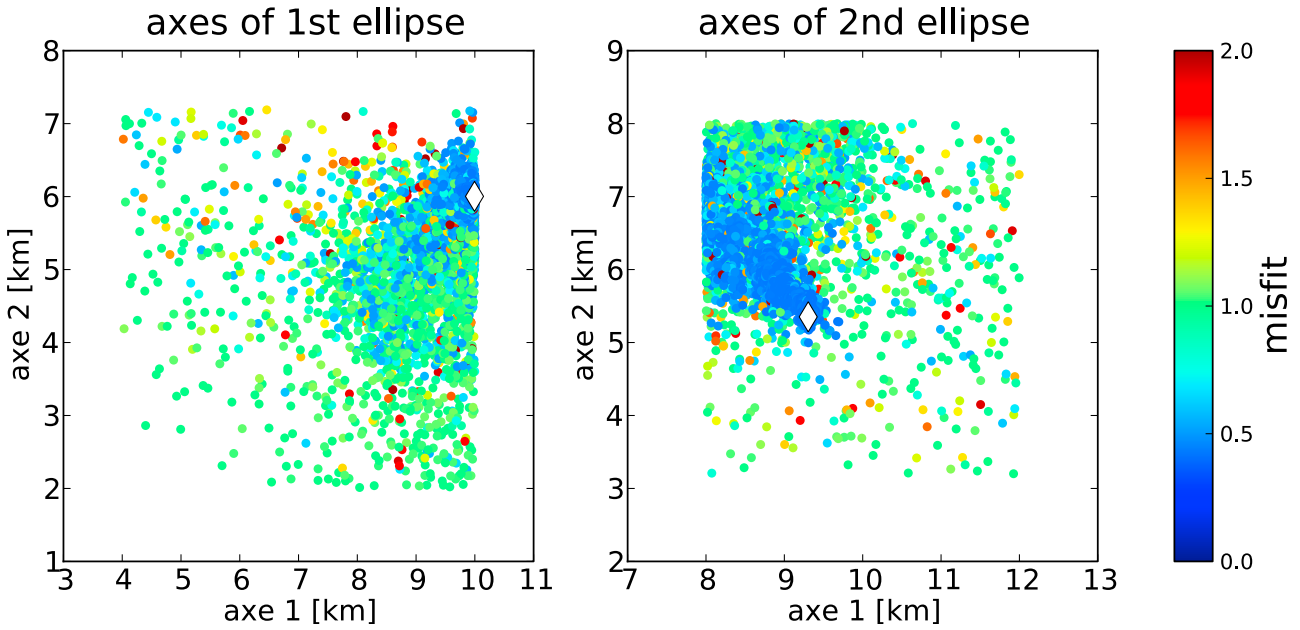

Figure 12. Convergence of dynamic inversion for model A. (left and right) Projection of model space onto the plane of semimajor axes of the two ellipses. The color scale indicates the goodness of fit of every sampled model. The best model, indicated by a white diamond, had a misfit of 0.399.

The stress drop computed by *Peyrat and Olsen* [2004], about 5 MPa on the average, is smaller than ours (10 MPa) because their fault surface was larger than the one we found.

6.2. Resolving Power of the Inversion Process

[37] The models generated by the inversion algorithm can be used to explore the properties of the solution of the inversion process. A much better method would be to do a Monte Carlo study of models near the optimum one, but this is impossible at present. For this reason we settled on an approach proposed by *Sambridge* [1999b]. We used the models visited by NA in order to generate plots of the distribution of these parameters. It is however very difficult to provide information about the resolution for 10 parameters, because there is no way to plot them.

[38] The simplest way to look at resolution is to study projections of the model space into lower dimensional subspaces. Since the parameter space for the two dynamic inversion has 10 dimensions there are many possible projections. Among them we chose those shown in Figures 12 and 13. In Figure 12 (left) we show the distribution of misfit function projected on the space of the axes of ellipse 1, the shallower one. In Figure 12 (right) we show the error distribution projected on the space of the axes of the second ellipse. The values of the axes for model A, our best model, are indicated by the white diamond. The models that produce misfit functions less than 0.6 are plotted by dark dots. For both ellipses we observe that the axes are well determined, although for the first ellipse one of the axes was chosen near the limit of the parameter range that we allowed to be explored. We did not allow for bigger values of a_1 because then the ellipse near the surface would be extremely long. Since slip is bounced by the free surface, such long ellipses would not change the synthetics anyways. In Figure 13 we show the distribution of error projected on the space of position of the center of the ellipses. In this case both are well resolved although there is a clear trade off. The second ellipse was not allowed to move further than 2 km from the hypocenter. The overall conclusion of these plots is that there are many models that fit the data with error less than 50%. The distribution of error are not Gaussian and there are clear evidences of large errors for certain parameters. For instance, the positions of the ellipses can change significantly without affecting the error. There is a caveat, however, as these figures represent only models that were chosen by NA in its approach of the minimum. To get a more complete idea of the distribution of models that do not fit the data we would have to explore the areas that appear in white in these plots, but that is too expensive for the moment.

6.3. On the Elliptical Patch Approximation

[39] Two questions about the elliptical patch approximation that we used in dynamic inversion are (1) whether this method can be extended to other geometries and (2) how many parameters can be resolved.

[40] Concerning the first question, elliptical patches are just the lower-order approximation in the wavelet expansion of general surface distributions, so that any two-dimensional function in 2-D can in principle be expanded using elliptical patches. The obvious problem with such an expansion is that it may not be very efficient because of the large number of patches that may be required to model complex stress distributions. Rectangular patches may be a better approach but discontinuities at the border between rectangles must be smoothed. Which method is more efficient must be carefully explored in the future. Fortunately, for low-frequency inversions all we need to obtain good convergence of the algorithm is few superposed ellipses.

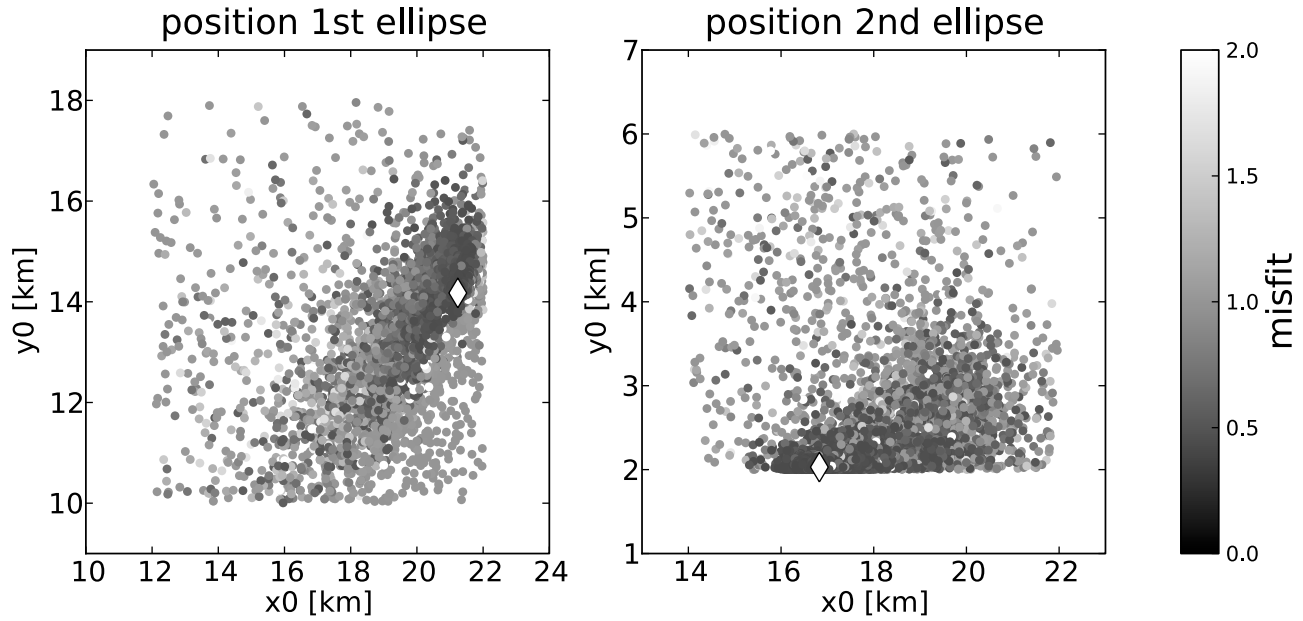

Figure 13. Convergence of dynamic inversion for model A. Projection of model space onto the plane of the positions of the center of the ellipses. The gray level indicates the goodness of fit of every sampled model. The best model, indicated by a white diamond, had a misfit of 0.399.

[41] As to the second question, nonlinear inversions are controlled by the number of independent parameters (degrees of freedom) actually contained in the data. In linear inversions the number of degrees of freedom is determined by the number of eigenvalues of the least squares matrix that are larger than a certain threshold. In this case it is possible to use functions approximated by a large number of rectangles, the number of degrees of freedom being reduced by numerical damping. In nonlinear inversion, when the direct problem is expensive, it is not possible to keep a large number of unresolved parameters in the inversion. Determining the actual number of effective degrees of freedom is thus very important. In the present work we could not determine the actual number of degrees of freedom because of limited computer resources, but we expect to be able to do this in the very near future. For the dynamic inversion of the Tottori earthquake we used only 10 independent parameters, the actual number of degrees of freedom is probably a little larger than 10, but not much. This may seem surprising, but it is the main reason why earthquake source inversions are often very nonunique.

7. Conclusions

[42] We used the strong motion data recorded in the vicinity of the Tottori fault to do nonlinear kinematic and dynamic inversion using the neighborhood algorithm (NA). Both inversions were based on the elliptical subfault approximation proposed by *Vallée and Bouchon* [2004]. We first did a kinematic inversion in order to establish a priori information that was later used to define the parameter range of dynamic inversion. In the second part, a direct non linear dynamic rupture inversion using the NA was computed. The spontaneous rupture process was computed numerically on a box surrounding the simplified fault of the Tottori earthquake. We used a barrier model to control rupture propagation. The initial stress was homogeneous except for a small asperity at the hypocenter used as a seed to start rupture. Friction was modeled by a couple of elliptical-shaped barriers. This dynamic rupture inversion method is fast because the number of independent parameters is low. Only ten parameters were inverted for in our problem, yet the models that we get fit the data very well at low frequencies. The technique proposed here can be extended to any number of elliptical patches. We have shown that for the Tottori earthquake two elliptical patches are sufficient to reproduce the rupture process. How many elliptical patches are actually needed to fully describe an earthquake? This of course depends on the number of seismograms available and their frequency band. For small events a single patch may be sufficient, providing average values of dynamic parameters. For earthquakes such as Tottori, we expect that two to three elliptical patches may be resolved. To conclude, these results have shown that dynamic inversion is possible with today computer resources. Depending on the improvement in available computer resources increasingly realistic dynamic inversions will become possible. Our results also illustrate a fundamental nonuniqueness of dynamic inversion.

[43] **Acknowledgments.** This work was supported by the SPICE project (contract MRTN-CT-2003-504267) of the European Commission Human Resources and Mobility Program and the Seismulators project of the CATEL program of Agence National pour la Recherche, ANR. We thank the National Research Institute for Earth Science and Disaster Prevention for the strong motion data. We thank Martin Mai and two anonymous referees for their very useful reviews of earlier versions of this paper.

References

Aki, K. (1979), Characterization of barriers on an earthquake fault, *J. Geophys. Res.*, *84*(B11), 6140–6148.

Backus, G., and M. Mulcahy (1976a), Moment tensors and other phenomenological descriptions of seismic source—I. Continuous displacements, *Geophys. J. R. Astron. Soc.*, *46*, 341–361.

Backus, G., and M. Mulcahy (1976b), Moment tensors and other phenomenological descriptions of seismic source—II. Discontinuous displacements, *Geophys. J. R. Astron. Soc.*, *47*, 301–329.

Bouchon, M. (1981), A simple method to calculate Greens function for layered media, *Bull. Seismol. Soc. Am.*, *71*, 959–971.

Bouchon, M., M. Campillo, and F. Cotton (1998), Stress field associated with the rupture of the 1992 Landers, California, earthquake and its implication concerning the fault strength at the onset of the earthquake, *J. Geophys. Res.*, *103*, 21,091–21,097.

Bukchin, B. G. (1995), Determination of stress glut moments of total degree 2 from teleseismic surface wave amplitude spectra, *Tectonophysics*, *248*, 185–191.

Cotton, F., and M. Campillo (1995), Frequency domain inversion of strong motions-application to the 1992 Landers earthquake, *J. Geophys. Res*, *100*(B3), 3961–3975.

Cotton, F. and O. Coutant (1997), Dynamic stress variations due to shear faults in a plane-layered medium, *Geophys. J. Int.*, *128*, 676–688.

Dalguer, L. A., K. Irikura, and W. Zhang (2002), Distribution of dynamic and static stress changes during 2000 Tottori (Japan) earthquake: Brief interpretation of the earthquake sequences; Foreshock, mainshock and aftershocks, *Geophys. Res. Lett.*, *29*(16), 1758, doi:10.1029/2001GL014333.

Das, S., and K. Aki (1977), Fault plane with barriers: A versatile earthquake model, *J. Geophys. Res.*, *82*(36), 5658–5670.

Fukuyama, E., and T. Mikumo (1993), Dynamic rupture analysis: Inversion for the source process of the 1990 Izu-Oshima, Japan, earthquake (M = 6.5), *J. Geophys. Res.*, *98*(B4), 6529–6542.

Fukuyama, E., W. L. Ellsworth, F. Waldhauser, and A. Kubo (2003), Detailed fault structure of the 2000 western Tottori, Japan, earthquake sequence, *Bull. Seismol. Soc. Am.*, *93*, 1468–1478.

Guatteri, M., and P. Spudich (2000), What can strong-motion data tell us about slip-weakening fault friction laws?, *Bull. Seismol. Soc. Am.*, *90*, 98–116.

Gusev, A. A., and V. M. Pavlov (1988), Determination of space time structure of a deep earthquake source by means of power moments, *Tectonophysics*, *152*, 319–334.

Hartzell, S. H., and T. H. Heaton (1983), Inversion of strong ground motion and teleseismic waveform data for the fault rupture history of the 1979 Imperial Valley, California, earthquake, *Bull. Seismol. Soc. Am.*, *73*, 1553–1583.

Ida, Y. (1972), Cohesive force across tip of a longitudinal-shear crack and Griffith's specific surface energy, *J. Geophys. Res.*, *77*(20), 3796–3805.

Ide, S., and M. Takeo (1997), Determination of constitutive relations of fault slip based on seismic waves analysis, *J. Geophys. Res.*, *102*, 27,379–27,391.

Iwata, T., and H. Sekiguchi (2002), Source process and near-source ground motion during the 2000 Tottori-ken Seibu earthquake, paper presented at 11th Japan Earthquake Engineering Symposium, Earthquake Eng. Res. Liaison Comm., Sci. Counc. of Jpn., Tokyo.

Kanamori, H., and G. S. Stewart (1978), Seismological aspects of the Guatemala earthquake of February 4, 1976, *J. Geophys. Res.*, *83*(B7), 3427–3434.

Kennet, B. L. N., and N. J. Kerry (1979), Seismic waves in a stratified half space, *Geophys. J. R. Astron. Soc.*, *57*, 557–583.

Madariaga, R. (1979), On the relation between seismic moment and stress drop in the presence of stress and strength heterogeneity, *J. Geophys. Res.*, *84*(B5), 2243–2250.

Madariaga, R., and K. B. Olsen (2000), Criticality of rupture dynamics in 3-D, *Pure Appl. Geophys.*, *157*, 1981–2001.

Madariaga, R., K. B. Olsen, and R. Archuleta (1998), Modeling dynamic rupture in a 3D earthquake fault model, *Bull. Seismol. Soc. Am.*, *88*, 1182–1197.

McGuire, J. J., L. Zhao, and T. H. Jordan (2001), Teleseismic inversion for the second-degree moments of earthquake space-time distributions, *Geophys. J. Int.*, *145*, 661–678.

Mikumo, T., and E. Fukuyama (2006), Near-source released energy in relation to fracture energy on earthquake faults, *Bull. Seismol. Soc. Am.*, *96*, 1177–1181.

Mikumo, T., K. B. Olsen, E. Fukuyama, and Y. Yagi (2003), Stress-breakdown time and slip-weakening distance inferred from slip-velocity functions on earthquake faults, *Bull. Seismol. Soc. Am.*, *93*, 264–282.

Monelli, D., P. M. Mai, S. Jonsson, and D. Giardini (2009), Bayesian imaging of the 2000 western Tottori (Japan) earthquake through fitting of strong motion data and GPS data, *Geophys. J. Int.*, *176*, 135–150.

Olsen, K. B., R. Madariaga, and R. J. Archuleta (1997), Three-dimensional dynamic simulation of the 1992 Landers earthquake, *Science*, *278*, 834–838.

Peyrat, S., and K. B. Olsen (2004), Nonlinear dynamic rupture inversion of the 2000 western Tottori, Japan, earthquake, *Geophys. Res. Lett.*, *31*, L05604, doi:10.1029/2003GL019058.

Peyrat, S., K. B. Olsen, and R. Madariaga (2001), Dynamic modeling of the 1992 Landers earthquake, *J. Geophys. Res.*, *106*(B11), 26,467–26,482.

Piatanesi, A., A. Cirella, P. Spudich, and M. Cocco (2007), A global search inversion for earthquake kinematic rupture history: Application to the 2000 western Tottori, Japan earthquake, *J. Geophys. Res.*, *112*, B07314, doi:10.1029/2006JB004821.

Pulido, N., and T. Kubo (2004), Near-fault strong motion complexity of the 2000 Tottori earthquake (Japan) from a broadband source asperity model, *Tectonophysics*, *390*, 177–192.

Sambridge, M. (1999a), Geophysical inversion with a neighbourhood algorithm—I. Searching a parameter space, *Geophys. J. Int.*, *138*, 479–494.

Sambridge, M. (1999b), Geophysical inversion with a neighbourhood algorithm—II. Appraising the ensemble, *Geophys. J. Int.*, *138*, 727–746.

Semmane, F., F. Cotton, and M. Campillo (2005), The 2000 Tottori earthquake: A shallow earthquake with no surface rupture and slip properties controlled by depth, *J. Geophys. Res.*, *110*, B03306, doi:10.1029/2004JB003194.

Vallée, M., and M. Bouchon (2004), Imaging coseismic rupture in far field by slip patches, *Geophys. J. Int.*, *156*, 615–630.

Yagi, Y., and K. Kikuchi (2000), Source process of the 2000 October 6 western Tottori earthquake (preliminary report)(in Japanese), *Newslett. Seismol. Soc. Jpn.*, *12*(4), 9–10.

S. Di Carli and R. Madariaga, Laboratoire de Géologie, CNRS-ENS, F-75231 Paris CEDEX 05, France. (sdicarli@geologie.ens.fr; madariag@geologie.ens.fr)

C. François-Holden, GNS Science, PO Box 30368, Lower Hutt 5040, New Zealand. (c.holden@gns.cri.nz)

S. Peyrat, Institut de Physique du Globe de Paris, F-75251 Paris CEDEX 05, France. (peyrat@ipgp.fr)